Morphological Stability and Performance of Polymer–Fullerene Solar Cells under Thermal Stress: The Impact of Photoinduced $PC_{60}BM$ Oligomerization

Him Cheng Wong,[†,§] Zhe Li,[‡,§] Ching Hong Tan,[‡] Hongliang Zhong,[‡] Zhenggang Huang,[‡] Hugo Bronstein,[‡] Iain McCulloch,[‡] João T. Cabral,[†,*] and James R. Durrant[‡,*]

[†]Department of Chemical Engineering, [‡]Department of Chemistry, Centre for Plastic Electronics, Imperial College London, London SW7 2AZ, United Kingdom. [§]Equal contribution.

ABSTRACT We report a general light processing strategy for organic solar cells (OSC) that exploits the propensity of the fullerene derivative $PC_{60}BM$ to photo-oligomerize, which is capable of both stabilizing the polymer:$PC_{60}BM$ active layer morphology and enhancing the device stability under thermal annealing. The observations hold for blends of $PC_{60}BM$ with an array of benchmark donor polymer systems, including P3HT, DPP-TT-T, PTB7, and PCDTBT. The morphology and kinetics of the thermally induced $PC_{60}BM$ crystallization within the blend films are investigated as a function of substrate and temperature. $PC_{60}BM$ nucleation rates on SiOx substrates exhibit a pronounced peak profile with temperature, whose maximum is polymer and blend-composition dependent. Modest illumination (<10 mW/cm^2) significantly suppresses nucleation, which is quantified as function of dose, but does not affect crystalline shape or growth, in the micrometer range. On PEDOT:PSS substrates, thermally induced $PC_{60}BM$ aggregation is observed on smaller (≈100 nm) length scales, depending upon donor polymer, and also suppressed by light exposure. The concurrent thermal dissociation process of $PC_{60}BM$ oligomers in blend films is also investigated and the activation energy of the fullerene–fullerene bond is estimated to be 0.96 ± 0.04 eV. Following light processing, the thermal stability, and thus lifetime, of PCDTBT:$PC_{60}BM$ devices increases for annealing times up to 150 h. In contrast, PCDTBT:$PC_{70}BM$ OSCs are found to be largely light insensitive. The results are rationalized in terms of the suppression of $PC_{60}BM$ micro- and nanoscopic crystallization processes upon thermal annealing caused by photoinduced $PC_{60}BM$ oligomerization.

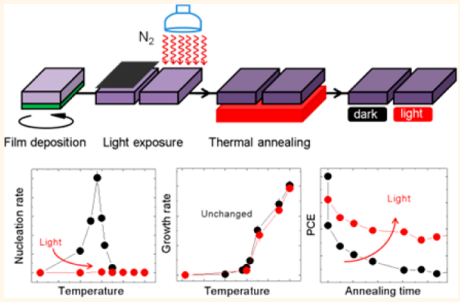

KEYWORDS: organic solar cells · PCBM photo-oligomerization · $PC_{60}BM$ crystallization · solar cell thermal stability and lifetime

Fullerenes have attracted great interest in both fundamental and applied research, since their discovery[1] and successful large-scale synthesis,[2] due to their promising optical and electronic properties. They are, however, known to be extremely light and oxygen sensitive, both in solution[3] and in the solid phase, either evaporated into neat fullerene films or blended with polymers. The photoinduced transformation of neat fullerenes (C_{60} and C_{70}) has been investigated since the early 1990s.[4] Upon exposure to UV or visible radiation, pristine fullerenes can be photopolymerized by forming covalent intermolecular C–C bonds between fullerene molecules through a '2 + 2' cycloaddition mechanism.[5] Oxygen greatly inhibits this process, attributed to O_2 molecules quenching the photoexcited triplet state, which is thought to be a necessary precursor to the photopolymerization process.[4,6] In addition, light exposure has been reported to greatly accelerate the diffusion of any present O_2 molecules into interstitial voids of the fullerene lattice in the neat solid phase, ultimately forming oxidized fullerene end-products instead.[4,6]

At present, fullerenes and their derivatives (PCBM) are ubiquitously used as active materials in numerous technological applications such as organic solar cells (OSCs), transistors and other electronic devices. In this work, we are concerned with the impact of light upon the thermal morphological behavior of solution processed polymer:

* Address correspondence to j.cabral@imperial.ac.uk, j.durrant@imperial.ac.uk.

Received for review September 6, 2013 and accepted January 8, 2014.

Published online January 08, 2014
10.1021/nn404687s

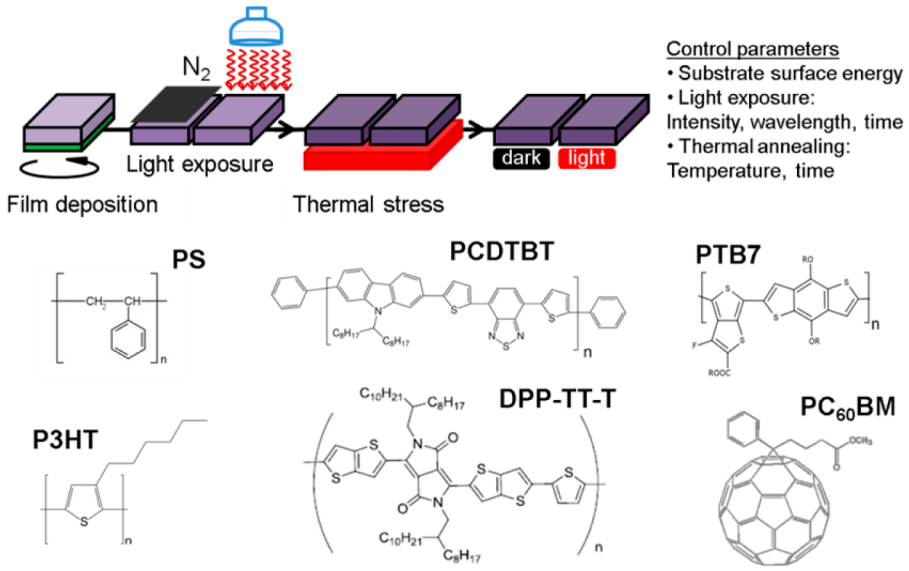

Figure 1. Schematic representation of the adopted light processing methodology and relevant control variables. Blend films or devices, without or with illumination, are represented as 'dark' and 'light', respectively, throughout this paper. Light exposure and the subsequent annealing steps in the present study were conducted in a nitrogen environment. A modest fluorescent light source with irradiance ≈10 mW/cm^2 was employed throughout most of this study, while an UV-A light (365 nm, 2.5 mW/cm^2) was used in comparative device studies. Chemical structures of the polymer repeat units and $PC_{60}BM$ are shown.

PCBM blends employed in OSCs. The fabrication of such OSC generally involves the phase separation and crystallization of active components, typically a stiff conjugated polymer and a fullerene derivative, within supported thin films obtained through a nonequilibrium deposition process, such as flow or spin coating. The control of phase separation morphology and crystalline structure of the heterogeneous films should thus be given more consideration, just like power conversion efficiency (PCE) and other device parameters in designing OSCs of better performance, reliability and lifetime.[7]

While C_{60} can form relatively long polymeric structures under illumination (in the absence of oxygen), phototransformation of its solution processable derivative $PC_{60}BM$ ([6,6]-phenyl-C61-butyric acid methyl ester) results in dimeric or oligomeric structures.[8−10] Regardless of the extent of polymerization, both phototransformed C_{60} and $PC_{60}BM$ have lower solubility in organic solvents compared to their pristine state.[4,10] Some research efforts have since focused on phototransformed neat $PC_{60}BM$ films, whose insoluble state and retained electronic properties allow for selective area solution processing and patterning of field-effect transistor arrays.[8,10]

We previously reported that C_{60} fullerenes can also undergo photochemical transformation when blended within styrenic and acrylic polymers, and this process is effective in suppressing film dewetting and affects, nontrivially, the C_{60} association and crystallization upon thermal annealing.[11] Further, we recently evaluated the impact of the photoinduced transformation to the performance of a model OSC system.[12] Modest light exposure was found to induce significant $PC_{60}BM$ transformation within carbazole donor polymer poly-[[9-(1-octylnonyl)-9*H*-carbazole-2,7-diyl]-2,5-thiophenediyl-2,1,3-benzothiadiazole-4,7-diyl-2,5-thiophenediyl] (PCDTBT) blend films, stabilizing blend morphology, and improving device performance and lifetime upon thermal annealing. An analogous increase in film morphological stability following irradiation has also been reported by Piersimoni *et al.*[13] on P3HT and MDMO-PPV blended with $PC_{60}BM$, and PCDTBT:$PC_{70}BM$, although device performance changes were not evaluated.

In this paper, we quantify the morphological implications of "light processing", illustrated schematically in Figure 1, and evaluate the generality of this approach as means to improving the thermal stability and performance of OSCs. We focus in particular on the analysis of mechanism and kinetics of thermally induced $PC_{60}BM$ crystallization and its significant suppression caused by light-induced $PC_{60}BM$ oligomerization. The approach is tested on a range of benchmark polymer:fullerene OSCs, namely, P3HT, DPP-TT-T, PTB7, and PCDTBT:$PC_{60}BM$ blends, chemical structures shown in Figure 1. The effect of illumination on the long-term OSC thermal stability is also examined, as well as the effect of the supporting substrate on film morphology, specifically contrasting silicon oxide (SiOx) and PEDOT:PSS (poly(3,4-ethylenedioxythiophene) poly(styrenesulfonate)), which is usually used as hole transport layer in OSC.

Our findings demonstrate that light processing can be employed as a performance-enhancing fabrication step, call into question the relevance of dark thermal

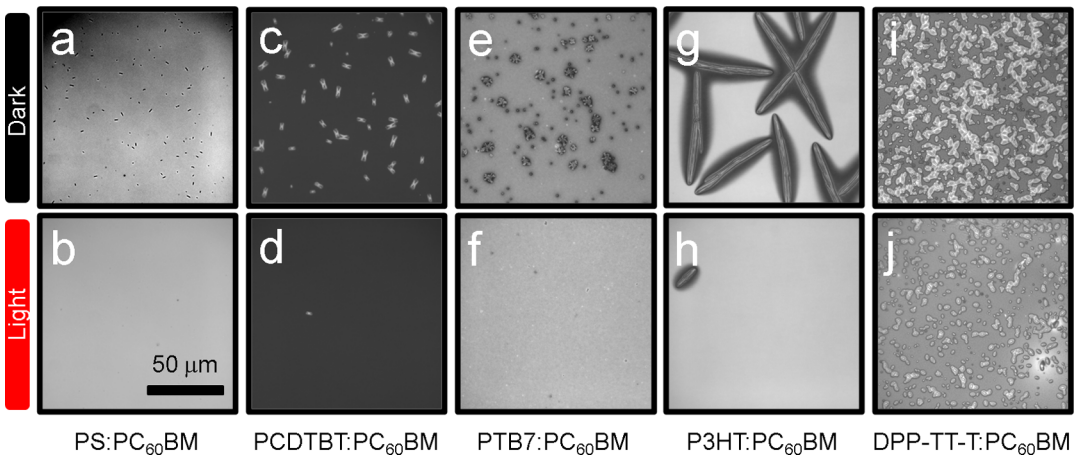

Figure 2. Optical microscopy images showing annealed morphologies of polymer:$PC_{60}BM$ blend films on SiOx substrates with (bottom row) and without (top row) prior light exposure. (a and b) PS:$PC_{60}BM$ (1:1); (c and d) PCDTBT:$PC_{60}BM$ (1:2); (e and f) PTB7:$PC_{60}BM$ (1:2); (g and h) P3HT:$PC_{60}BM$ (1:2); (i and j) DPP-TT-T:$PC_{60}BM$ (1:2). Films at bottom panel were exposed to fluorescent light (10 mW/cm^2) for 165 min prior to annealing. PS, PCDTBT, and PTB7 blend films were annealed at 140 °C for 60 min, and P3HT and DPP-TT-T blend films were annealed at 140 °C for 6 min. Film thicknesses vary from 70 to 120 nm and are identical for each dark and light polymer film pair.

stress stability studies as an assay of device durability, and finally indicate that light exposure should at any rate be monitored in order to ensure reproducibility of device and morphological results, as illumination prior to thermal stress affects polymer:fullerene blends in a nontrivial manner.

RESULTS AND DISCUSSION

Light-Induced Suppression of $PC_{60}BM$ Crystallization. We first consider the effect of light exposure on the thermally annealed morphology of various polymer:$PC_{60}BM$ blend films supported on high surface energy SiOx substrates (≈73 mN/m). We investigate $PC_{60}BM$ mixtures with an array of polymers, namely, PS; PCDTBT; PTB7; P3HT and DPP-TT-T. This range includes both amorphous and crystalline polymers, as well as significant variations in material energetics and optical bandgaps. The top row in Figure 2 shows that without light exposure, micrometer-sized $PC_{60}BM$ crystallization generally occurs during thermal annealing. On the other hand, the additional light processing prior to annealing drastically suppresses the formation of large-scale $PC_{60}BM$ crystals, resulting in largely uniform film morphologies except for DPP-TT-T which exhibits a more modest effect under these conditions, as illustrated in the bottom row of Figure 2. The results can be rationalized in terms of $PC_{60}BM$ oligomerization induced by light processing, discussed below, which evidently affects molecular diffusion properties during annealing. The $PC_{60}BM$ phototransformation process is general for all polymer:$PC_{60}BM$ OSC blends we have studied so far, and it can significantly influence their morphological properties.

In the absence of light exposure, $PC_{60}BM$ crystallizes upon annealing at 140 °C within 3−6 min in semicrystalline P3HT and DPP-TT-T blends and approximately 1 h in amorphous PCDTBT, PTB7, and PS blends, whose glass transition temperatures (T_g) range from 12 °C (P3HT) to 106 °C (PCDTBT). Regardless of quench depth (ΔT = 140 °C − T_g), considerable (or complete) crystallization suppression is found for all polymers, as shown in Figure 2.

Selecting PCDTBT:$PC_{60}BM$ as a benchmark model system, we next examine the mechanism and kinetics of thermally induced $PC_{60}BM$ crystallization and its suppression by light exposure. Optical microscopy images in Figure 3 highlight the influence of light exposure on the nucleation and growth of $PC_{60}BM$ microscopic crystals in blends with PCDTBT as a function of annealing temperature. The insets show a magnified view of the $PC_{60}BM$ crystals, showing the evolution of their size and shape at various annealing temperatures, with and without prior light processing. A change in the shape of $PC_{60}BM$ crystals (from 'chromosome-like' to 'needle-like') was observed above 160 °C which can be interpreted as a suppression of secondary nucleation and crystal branching with increasing temperature, possibly associated with a reduction in surface tension anisotropy.[14]

We next investigate the nucleation and growth kinetics of the microscopic $PC_{60}BM$ crystals within the polymer matrix as a function of temperature. Optical microscopy images in Figure 4a−e show their time evolution at 143 °C from which the nucleation density (Nd) and average crystal length ⟨d⟩ are extracted and plotted in Figure 4, panels f and g, respectively. The temperature dependence of the nucleation and growth rates, estimated from the initial change of crystal Nd and ⟨d⟩ per unit time (*i.e.*, slope of the curve), are plotted in Figure 4h,i.

In Figure 4h, the nucleation rate for films in our control experiment (*i.e.*, without light exposure, black

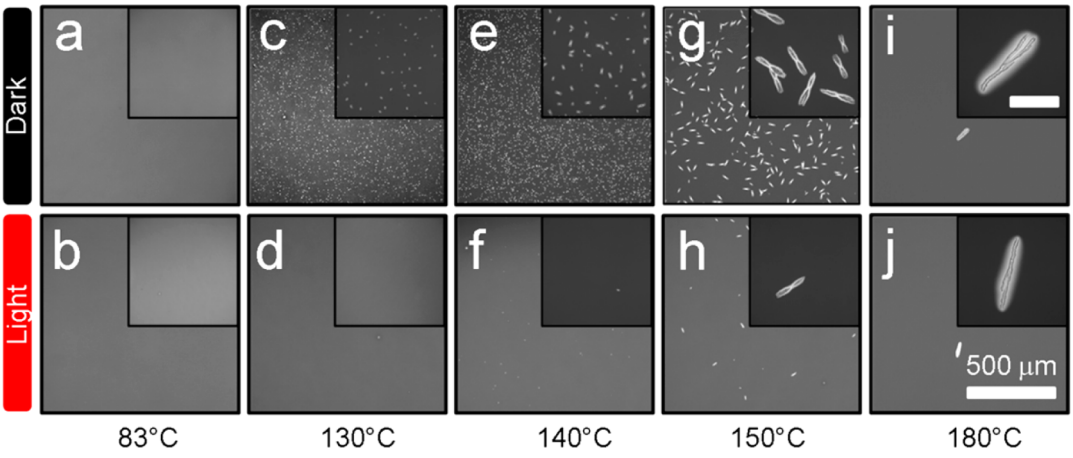

Figure 3. Temperature dependence of $PC_{60}BM$ nucleation and growth in PCDTBT:$PC_{60}BM$ (1:2) blend films (thickness = 80 ± 3 nm) on SiOx substrates, annealed for 60 min at the indicated temperatures. Magnified insets show the evolution of $PC_{60}BM$ crystal number density, size, and shape at various annealing temperature. Inset scale bar: 50 μm. Films in the bottom row were exposed to fluorescent light (10 mW/cm^2, 165 min) prior to annealing.

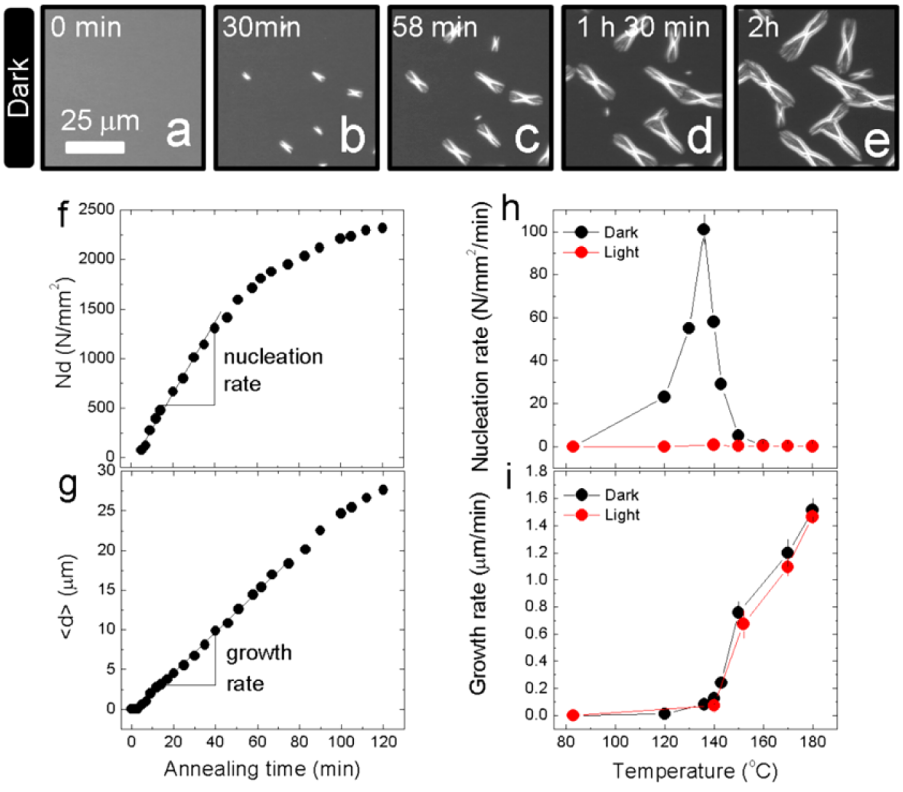

Figure 4. (a–e) Optical micrographs showing $PC_{60}BM$ nucleation and growth kinetics (illustrated for 143 °C) in PCDTBT:$PC_{60}BM$ (1:2) blend film on SiOx substrates, and obtained nucleation density Nd, average crystal length ⟨*d*⟩ and the corresponding rates (f and g). $PC_{60}BM$ (h) nucleation (Nd) and (i) growth (⟨*d*⟩) rate analysis of PCDTBT:$PC_{60}BM$ (1:2) films on SiOx as a function of annealing temperature. Fluorescent light exposure (10 mW/cm^2, 165 min) strongly suppresses $PC_{60}BM$ nucleation but does not measurably affect growth upon thermal annealing.

symbols) is found to peak around 140 °C and then to drop abruptly thereafter. In contrast, the nucleation rates for illuminated blend films (red symbols) are significantly suppressed across all temperatures investigated. On the other hand, the growth rate exhibits a monotonic increase with increasing annealing temperature, with no measurable change in average crystal length for films exposed to light, within experimental uncertainty, as shown in Figure 4i and insets of Figure 3. The photo-oligomerization process appears thus to affect the nucleation process (and hence the crystal density), and do so dramatically, but not the crystal growth.

The decrease in $PC_{60}BM$ nucleation rate in unilluminated films takes place around 140 °C, which is far below its neat melting temperature of 285 °C, see

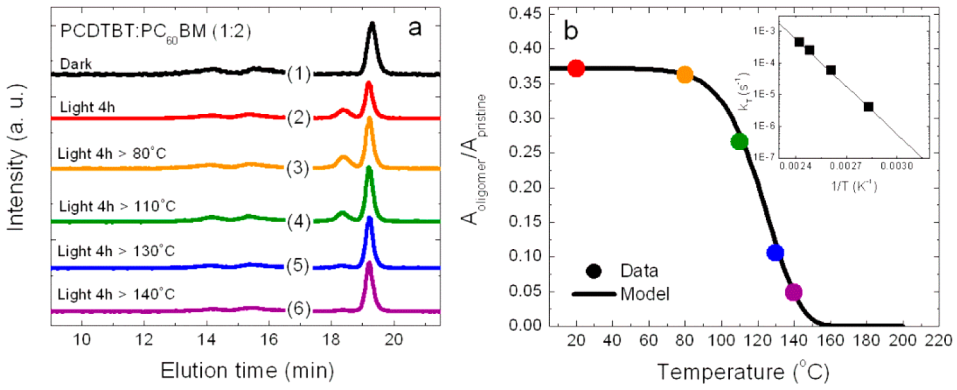

Figure 5. (a) Gel permeation chromatography (GPC) traces of redissolved PCDTBT:$PC_{60}BM$ (1:2) blend films without (1) and following (2) fluorescent light exposure (10 mW/cm^2, 240 min). Traces (3)−(6) are GPC data of illuminated blend films subjected to subsequent thermal annealing (in the dark) for 60 min at various temperatures. (b) Ratio between $PC_{60}BM$ oligomer and pristine $PC_{60}BM$ population, based on GPC area fraction analysis, as a function of temperature. The solid line is a model fit (see text) and graph inset is an Arrhenius plot of the thermal dissociation rate constant k_T from which activation energy E_A of 0.96 ± 0.04 eV is estimated.

Supporting Information Figure S1. According to classical crystallization theory,[15,16] the crystallization of a single component material drops when approaching its melting point. This observation is thus likely to be due to the reduced melting point of $PC_{60}BM$ in the blend, by approximately 100−150 °C as found in P3HT:$PC_{60}BM$.[17] The increased side chain ordering transition in PCDTBT[18−20] at ≈140 °C is unlikely to contribute to the reduced $PC_{60}BM$ nucleation rate because similar behavior is observed when $PC_{60}BM$ is blended with amorphous polystyrene (see Supporting Information Figure S2).

Thermal Dissociation of Photo-Oligomerized $PC_{60}BM$. Evidence of $PC_{60}BM$ oligomerization is provided by gel permeation chromatography (GPC), as we have shown previously.[12] Pure components PCDTBT and $PC_{60}BM$ appear at elution times 14−16 and 19.3 min, respectively. Traces (1) and (2) in Figure 5a demonstrate that a larger species emerges upon illumination (10 mW/cm^2, 240 min) at approximately 18.4 min elution time, corresponding to 2−3 $PC_{60}BM$ monomer units. The majority of $PC_{60}BM$, however, remained pristine. The photo-oligomerized $PC_{60}BM$ species within the film is relatively stable at room temperature in N_2 atmosphere as unchanged traces are obtained for blend films tested one month after light treatment (data not shown).

It has been previously reported that thermal energy can break the covalent bonds between the photopolymerized C_{60}, reverting them back to their pristine state above 100 °C.[4,21] To establish the thermal stability of phototransformed $PC_{60}BM$ species in OSC blend film, we estimate the onset temperature of $PC_{60}BM$ thermal deoligomerisation by monitoring the disappearance of the oligomer peak. GPC measurements were carried out on solutions obtained from dissolution of illuminated PCDTBT:$PC_{60}BM$ blend films subsequently annealed for 60 min at various temperatures. To exclude sample preparation artifacts in the results, several redissolution methods were attempted. We find that the GPC oligomer peak intensity is invariant for films redissolved with the aid of sonication for up to 30 min or by merely mechanical stirring; the latter is adopted in this study. The results confirm that the $PC_{60}BM$ oligomer population formed upon irradiation has not been affected by the dissolution step, thus adding confidence to our obtained results.

Traces (2)−(6) in Figure 5a characterize the reduction in the $PC_{60}BM$ oligomer peak with increasing temperature at constant annealing time (60 min). To estimate the population ratio of oligomer *vs* pristine $PC_{60}BM$, we compute the GPC area fraction of oligomer and pristine $PC_{60}BM$ peaks ($A_{oligomer}/A_{pristine}$) in Figure 5b. The graph quantifies the extent of thermal deoligomerisation of phototransformed $PC_{60}BM$ at constant time, showing that the $PC_{60}BM$ deoligomerisation initiates at ≈85 °C, with almost all $PC_{60}BM$ oligomers thermally reversed at ≥150 °C, in close agreement with C_{60} data.[4,21]

We model the population ratio of $PC_{60}BM$ oligomers and monomers with a simple rate equation successfully used to describe the thermal dissociation of C_{60} by Wang *et al.*[21] and detailed in Appendix. The solid line in Figure 5b corresponds to a model fit to eq 4 in Appendix and shows good agreement with the data. The rate constant of the thermal dissociation of $PC_{60}BM$ oligomer k_T is found to exhibit Arrhenius temperature dependence with activation energy E_A of 0.96 ± 0.04 eV (1.54 ± 0.06 × 10^{-19}J), see inset of Figure 5b. To the best of our knowledge, this is the first determination of the thermal dissociation activation energy of phototransformed $PC_{60}BM$. The value is slightly lower than the thermal energy previously reported to break a monomer from high intensity UV-photopolymerized C_{60} (1.25 eV).[21] This difference is likely to arise from steric hindrance[8] of $PC_{60}BM$ side chain which restricts the product of the photochemical process to dimers and oligomers, but we cannot at this

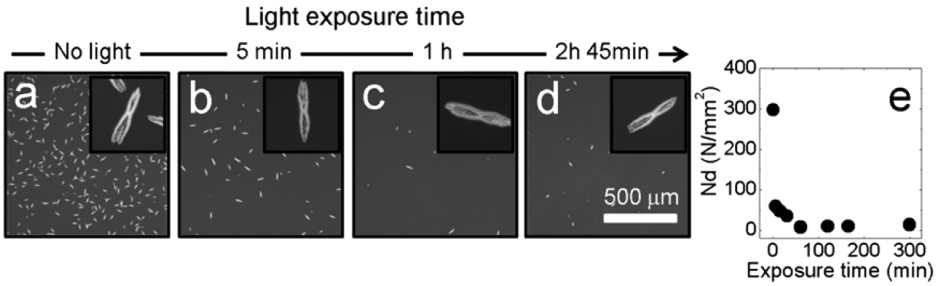

Figure 6. (a−d) Optical microscopy images of annealed PCDTBT:$PC_{60}BM$ (1:2) with increasing fluorescent illumination times (irradiance ≈ 10 mW/cm^2) prior to annealing at 150 °C for 60 min, showing about 5-fold drop in nucleation density (Nd), within 5 min (see e) but not size (see insets a−d). Inset image width: 50 μm.

stage rule out the effects of different incident radiation (wavelength and intensity), and polymer matrix. This activation energy lies in between typical energies for hydrogen and covalent bonds. The regular $PC_{60}BM$ thermal decomposition trend across the polymer glass transition suggests some independence of the process from polymer matrix mobility.

To quantify the light dose required to suppress $PC_{60}BM$ crystallization and stabilize the film morphology, we gradually vary exposure time and repeat the analysis above. The average crystal length $\langle d \rangle$ remains invariant with exposure time (see insets of Figure 6a−d). In fact, such crystals grow at the same rate regardless of illumination, corroborating earlier findings shown in Figure 4i (light *vs* dark). The $PC_{60}BM$ Nd, however, decreases about 5-fold in annealed films subjected to merely 5 min of light exposure and, for longer light exposure time (165 min), Nd drops 30 times (see Figure 6e), despite the presence of a relatively small oligomer fraction due to the thermal deoligomerisation process. We hypothesize that such microscopic crystals comprise solely $PC_{60}BM$ monomer and thus that light exposure reduces the fraction of monomers and thus spatially restricts the thermally activated nucleation step.

We rationalize the resulting morphologies in terms of the interplay between deoligomerisation and crystallization kinetics that happen simultaneously. At higher temperatures (≈140−150 °C), deoligomerisation takes place within crystallization time scales, and crystallization returns albeit with a much lower nucleation density. Indeed, the microscopic nucleation rate is approximately 70 times and 30 times smaller in illuminated *vs* dark films at 140 and 150 °C, respectively. At lower temperatures (≤130 °C), deoligomerisation is now slower compared to nucleation, which leads to full crystallization suppression within our annealing time scales. From the modeling of GPC results (Supporting Information Figure S3), the oligomer fraction decreases from approximately 30% to 10% (at 130 °C) within 60 min of annealing, and it thus appears that even such relatively low oligomer fraction is sufficient to prevent the nucleation of the predominant $PC_{60}BM$ monomers in these high-loading polymer:$PC_{60}BM$ films (1:2).

Substrate Dependence of Light Suppression of $PC_{60}BM$ Crystallization. Fullerene assembly and crystallization depends strongly on substrate and surface energy.[22−24] Our data above have so far been restricted to SiOx substrates. We next consider PEDOT:PSS substrates, given its ubiquitous use in enhancing hole extraction in OSCs. Typical data is shown in Figure 7. While 'chromosome-like' $PC_{60}BM$ microscopic crystals are clearly visible on SiOx surface (Figure 7b,c) upon annealing above T_g, markedly fewer microscopic crystals appear on PEDOT:PSS (Figure 7l,m).

The distinct $PC_{60}BM$ crystallization on both substrates can be rationalized in terms of the substrate surface energy dependent $PC_{60}BM$ depth profile[22−24] within the as-cast films. A recent spectroscopic ellipsometry study[23] on P3HT:$PC_{60}BM$ (1:1) system shows that $PC_{60}BM$ is more enriched on SiOx surfaces (73 mN/m) compared to the relatively hydrophobic PEDOT:PSS (47 mN/m). It has been shown in donor polymer:$PC_{60}BM$ blends that $PC_{60}BM$, the higher surface energy material (38 mN/m[22]), would preferentially wet the hydrophilic SiOx interface, while the lower surface energy donor polymers, for example, P3HT (27 mN/m[22]), reside more toward the relatively hydrophobic PEDOT:PSS surface upon spin coating. It was thus suggested[24] that such $PC_{60}BM$-rich layer on SiOx can accelerate the crystallization process, resulting in more microscopic $PC_{60}BM$ crystals on SiOx than on PEDOT:PSS substrates. $PC_{60}BM$ enrichment at the polymer−air interface was found for as-cast PCDTBT:$PC_{60}BM$ films on PEDOT:PSS.[25] Using neutron reflectivity (D17, Institut Laue-Langevin; *data not shown*), we have confirmed this result for our films and found that, by contrast, the $PC_{60}BM$ profile orthogonal to the film surface on SiOx is comparatively uniform; the fullerene concentration near the substrate is thus higher in the latter. The visible and UV light absorption of our 80 nm films is relatively low, ranging from 30 to 10% in the UV−vis range, indicating a small variation of light intensity normal to the film. We thus conclude that photo-oligomerization takes place following the $PC_{60}BM$ concentration depth profile, provided that the interparticle spacing satisfies the topochemical requirement, discussed next.

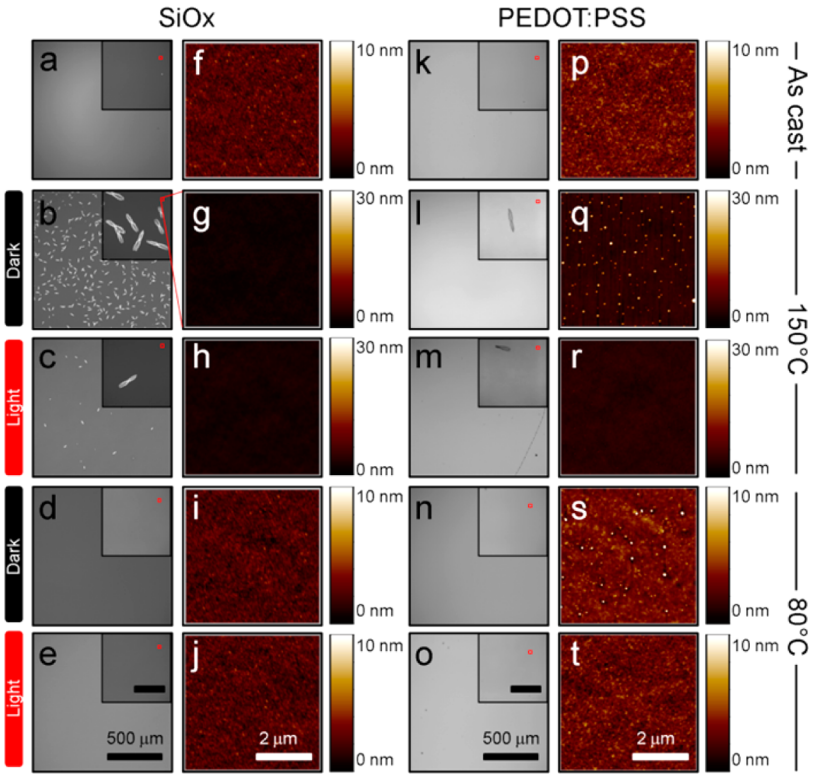

Figure 7. Optical microscopy images of as-cast and annealed (1 h) PCDTBT:$PC_{60}BM$ (1:2) films on SiOx and PEDOT:PSS surfaces (scale bars: 500 and 50 μm for inset). AFM images are shown on the right side of the corresponding optical images, comparing the effect of fluorescent light exposure (10 mW/cm^2, 165 min) on submicrometer annealed morphologies. The red box in each inset represents the AFM scan area for each condition.

At 150 °C, both unilluminated and light-treated blend films on PEDOT:PSS exhibit few microscopic $PC_{60}BM$ crystals (see Figure 7l,m) and optical microscopy becomes insufficient to gauge the light induced crystallization suppression. Atomic force microscopy (AFM) reveals $PC_{60}BM$ features of the order of 150 nm in diameter and 30 nm in height present in unilluminated annealed samples (Figure 7q). On the other hand, annealed films subjected to prior light exposure show substantially stabilized morphology with smaller and sparse $PC_{60}BM$ features, see Figure 7r and Supporting Information Figure S4. Like the as-cast morphology (Figure 7a,f), nanoscale crystals are not observed in both dark and light treated blend films on SiOx at 150 °C (Figure 7g,h) and 80 °C (Figure 7i,j). Formation of nanoscale $PC_{60}BM$ aggregates was observed on PEDOT:PSS following annealing at 80 °C (Figure 7s). At this temperature, microscopic $PC_{60}BM$ microcrystals are absent on PEDOT:PSS (Figure 7n,o) as well as on SiOx (Figure 7d,e). Prior light exposure was again observed to suppress $PC_{60}BM$ crystallization/aggregation (Figure 7t), resembling as cast morphology (Figure 7k,p), thus demonstrating the impact of light exposure upon film morphological stability under conditions relevant to practical OSC operating conditions.

A bimodal distribution of $PC_{60}BM$ crystal population and size in blends with PS has been previously reported on mica substrates.[26] Depending on annealing temperature, large needle-like $PC_{60}BM$ crystals ($\approx$10 μm in length) are gradually replaced with smaller $\approx$1-μm-cubic-aggregates, whose crystalline structure was verified by selected area electron diffraction (SAED).[26] In contrast, needle-like crystallites are observed on PS: $PC_{60}BM$ on glass. The thermally induced $PC_{60}BM$ crystallization is thus evidently substrate dependent, due to the combined effects of surface segregation and possible epitaxial growth. In PCDTBT blends on SiOx, the dominant length scale of $PC_{60}BM$ crystallization is in the micrometer range, while on PEDOT:PSS, it is in the nanometer range. In both cases, prior light exposure suppresses or reduces crystal formation, depending on annealing temperature.

In contrast to PCDTBT:$PC_{60}BM$ blend films, we observed micrometer-sized $PC_{60}BM$ crystals on both SiOx and PEDOT:PSS surfaces above T_g for both P3HT:$PC_{60}BM$ and PTB7:$PC_{60}BM$ blend films (both 1:2 polymer to $PC_{60}BM$ ratio) (see Supporting Information Figure S5). It is likely that this difference in length scale of thermally induced $PC_{60}BM$ crystallization is related to the miscibility and microstructure of these blend films; we note, for example, that both P3HT and PTB7 exhibit optimum OSC performance at lower $PC_{60}BM$ blend compositions than PCDTBT.[17,27] However in all cases, independently of the length scale of $PC_{60}BM$ crystallization, prior light exposure was observed to

suppress thermally induced $PC_{60}BM$ crystal formation (see Supporting Information Figure S5).

The microscopic crystallization suppression effect was observed to require a system-dependent threshold $PC_{60}BM$ loading in order to have adequate sensitivity to illumination. In particular, light processing does not affect the annealed morphology of P3HT:$PC_{60}BM$ (1:0.8) blend films (without prior thermal processing) but proved to be effective in P3HT:$PC_{60}BM$ (1:2) blend films, see Figure 2g,h. At higher loading, more $PC_{60}BM$ arrangements can be expected to satisfy the general topochemical requirement[4] (*i.e.*, parallel carbon double bond alignment of adjacent $PC_{60}BM$ and less than 4.2 Å apart) for photo-oligomerization to occur. The threshold loading, however, depends on the polymer−fullerene miscibility (and thus their interaction and orientation); for example, PS:$PC_{60}BM$ (1:1) exceeds the threshold for morphology stabilization (see Figure 2a,b). The crystallization suppression at relatively low oligomer:monomer fractions, of the order of 1:10 to 1:3, is thus likely due to the hindered thermal activation and formation of critical $PC_{60}BM$ nuclei.

OSC Device Stability Enhancement by Light Processing. We now consider the effect of light exposure on the performance and stability of PCDTBT:$PC_{60}BM$ (1:2) devices with conventional configuration of ITO/PEDOT:PSS/active layer/Ca/Al. Blend films were illuminated before electrode deposition. The light exposure conditions employed were sufficiently low that they did not result in a significant loss of initial device efficiency (typically δ(PCE) $\approx \pm 5\%$), indicating that the PCBM photo-oligimersation induced by this treatment does not substantially impact upon device function, as we have discussed previously.[12] The completed devices were then annealed in a N_2 glovebox at 80 °C under dark conditions, and current density−voltage ($J-V$) characteristics were measured under AM1.5 simulated solar irradiation at 100 mW/cm^2 at regular time intervals. A temperature of 80 °C is chosen, as such testing temperature is typically used in device accelerated lifetime testing,[7,28] and shown to cause minimal $PC_{60}BM$ deoligomerisation by GPC (see Figure 5b).

Dark 80 °C thermal annealing of PCDTBT:$PC_{60}BM$ devices in the absence of prior light exposure (and with minimal light exposure during efficiency measurements) was observed to result in an initial rapid loss of efficiency (typically 15−20%) over the first 20−120 min (see Figure 8a,b, black circles), followed by a much slower decay over following 150 h (the longest time scale studied). This two-stage behavior is analogous to that reported previously.[29,30] The initial decay phase is on a similar time scale to the formation of $PC_{60}BM$ crystallites/aggregates in films reported above. Given our observation that prior light exposure can suppress this crystallization process, we focus particularly upon the potential for light exposure to suppress this decay phase of device thermal stability.

Figure 8a illustrates the PCDTBT:$PC_{60}BM$ (1:2) device stability as a function of illumination time prior to annealing at 80 °C. We observe that the device thermal stability systematically increases with light exposure time. Further, at a constant annealing time of 120 min, the PCE percentage retained increases linearly from 75% without light processing to approximately 90% at the plateau exposure time of ≈170 min (see inset of Figure 8a). Such plateau estimate concerns a fluorescent light source and fixed irradiance (10 mW/cm^2). $PC_{60}BM$ photo-oligomerization has been shown to depend on light intensity more than the illumination time,[9] the use of brighter light could thus significantly shorten the exposure time required to achieve the same degree of stabilization effect.

Since OSC degradation pathways can be linked to the temperature-induced electrode interfacial (delamination) issues and/or active layer morphological changes, additional experiments are needed to separate and indentify the dominant effects. To do that, we preclude the electrode from the annealing step by annealing the PCDTBT:$PC_{60}BM$ (1:2) devices at 80 °C before electrode deposition (preannealed). They are then compared to devices from the same batch similarly annealed after electrode deposition (postannealed). We show in Figure 8b that preannealed and postannealed devices show similar thermal stability behavior, and therefore show that the order of annealing and electrode deposition (which alters surface interactions) is unimportant. This applies to both dark and illuminated devices. The observation suggests that for the devices studied herein (a) dark device degradation under 80 °C thermal stress could originate from $PC_{60}BM$ diffusion into nanoscale structures rather than thermally induced electrode delamination, and (b) the light-induced suppression of such nanoscale crystals (see AFM images in Figure 7s,t) is likely to be the underlying factor in enhancing device thermal stability.

We show in Figure 8c that, with light processing, the enhancement of PCDTBT:$PC_{60}BM$ (1:2) device stability is maintained for time scales over 150 h at 80 °C, consistent with our earlier observation that this temperature is too low to drive significant thermally induced deoligomerization of $PC_{60}BM$. It is noted that our methodology involves illumination prior to device annealing while actual device operation is typically conducted under continuous irradiation.[31] We thus carried out device testing with simultaneous irradiation (4.5 mW/cm^2) and annealing over 150 h; an analogous device stabilization effect was also observed (see Supporting Information Figure S6), confirming the potential for continuous irradiation to stabilize film morphology. However, we have so far only undertaken such long-term irradiation studies at modest light fluxes; it has been widely reported that prolonged exposure to one sun intensities can result in

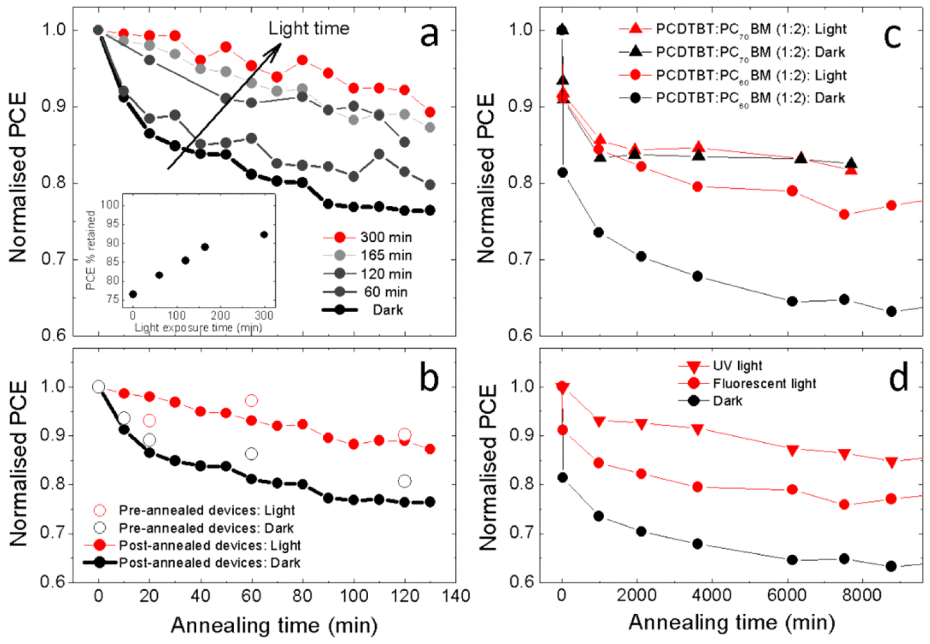

Figure 8. (a) Effect of illumination on PCDTBT:$PC_{60}BM$ (1:2) device stability under isothermal annealing; Inset shows the percentage of device PCE retained at constant testing time of 120 min with various fluorescent light exposure times. (b) Normalized PCE for illuminated (red) and dark (black) PCDTBT:$PC_{60}BM$ (1:2) devices annealed before (preannealed, unfilled) and after (postannealed, filled) electrode deposition. (c) Comparison of long-term device stability behavior of PCDTBT-based OSC with $PC_{60}BM$ (circles) and $PC_{70}BM$ (upward triangles). The average initial device PCE from five $PC_{60}BM$ and $PC_{70}BM$-containing devices is 5.5 $\pm$ 0.8% and 6.8 $\pm$ 0.4%, respectively. (d) Effect of illumination wavelength on PCDTBT:$PC_{60}BM$ (1:2) device annealing study. Light exposure was carried out before electrode deposition; exposure time was 165 min, unless otherwise indicated in (a). Annealing was conducted at 80 °C after electrode deposition except for unfilled data in (b). All light processing steps were carried out with a fluorescent light source (10 mW/cm^2) except for the downward triangles in (d) which correspond to a UV-A source (2.5 mW/cm^2).

additional degradation pathways[31−33] that are beyond the scope of the present study.

Recent literature[19,31,34,35] have reported that the use of $PC_{70}BM$ rather than $PC_{60}BM$ as electron acceptor can result in higher OSC efficiencies, although the technological potential of this acceptor is limited by its relatively higher cost. In order to evaluate the applicability of the light processing procedure with $PC_{70}BM$-containing OSC, comparative device stability experiments were performed on PCDTBT:$PC_{70}BM$ (1:2) OSCs, as shown in Figure 8c. C_{70} is known to be more difficult to photopolymerize, attributed to its relatively smaller number of reactive double bonds compared to C_{60}.[4,36] We indeed find that light processing results in only a marginal increase in the thermal stability for $PC_{70}BM$ devices, at least for the modest illumination and thermal stress conditions investigated. Consistent with this observation, optical microscopy indicated that prior light exposure results in only a marginal suppression of thermally induced $PC_{70}BM$ crystallization, while GPC measurements showed that only a relatively small fraction of $PC_{70}BM$ are oligomerized even after prolonged (16 h) light exposure (see Supporting Information Figure S7). It is also apparent from Figure 8c that unilluminated PCDTBT:$PC_{70}BM$ devices have superior thermal stability compared to analogous $PC_{60}BM$ devices, in agreement with studies of Wang *et al.*[35] This higher thermal stability may be related to the higher fullerene miscibility reported for PCDTBT:$PC_{70}BM$.[37] Consistent with these observations, our light microscopy morphological studies of the impact of dark thermal annealing indicate a higher temperature (≈140−150 °C) is required to induce $PC_{70}BM$ crystallization in comparison with $PC_{60}BM$ (see Supporting Information Figure S7).

We finally explore different wavelengths of light in the device light processing (see Supporting Information Figure S8 for light spectra). In Figure 8d, we show that PCDTBT:$PC_{60}BM$ (1:2) devices exposed to lower wavelength UV-A light (2.5 mW/cm^2) show greater thermal stability improvement compared to fluorescent light exposure (10 mW/cm^2 visible light), consistent with the relatively strong absorbance of PCBM in the UV-A spectral region. The stability enhancement by UV-A is however accompanied with a larger (≈12%) drop in initial device PCE. Previous literature[38,39] indeed report that excessive chemical cross-linking can often lead to both enhanced stability and compromised initial device performance.

The results reported here correspond to relatively modest fluorescent light exposures (typically 2 h at 10 mW/cm^2). Such exposures resulted in only small or negligible loss of device efficiency (typically δ(PCE) ≤ 5%), demonstrating that modest light exposure can be

employed to enhance film morphological stability without substantially compromising device function and electronic properties, evidenced by negligible changes of UV−vis absorption and photoluminescence.[12] It has, however, been widely reported that more prolonged or intense light irradiation can result in more substantial loss of device efficiency.[31−33] For example, Distler *et al.* have recently reported[32] a study of OSC devices based on blends of a thiazole based donor polymer with $PC_{60}BM$, where 5 h of one sun irradiation resulted in an ≈20% loss of device efficiency, and suggested this loss may result from excessive $PC_{60}BM$ dimerization. As such, the results reported herein should not be taken as implying that light exposure will in general enhance OSC performance and stability, but rather that light exposure can have a beneficial impact on one aspect of this performance, namely, the morphological stability of the photoactive layer under thermal stress.

CONCLUSIONS

In summary, light induced $PC_{60}BM$ oligomerization is shown to be capable of significantly stabilizing the morphology of a range of polymer:$PC_{60}BM$ blend films. Our results are robust to both flexible (PS) and benchmark OSC conjugated polymers (P3HT, PCDTBT, PTB7, DPP-TT-T). On SiOx substrates, exposure to visible light affects thermally driven $PC_{60}BM$ nucleation processes, causing a rapid decrease of the number density of $PC_{60}BM$ microcrystals, without impacting upon the growth kinetics of the microcrystallites. On lower surface energy PEDOT:PSS surfaces, thermal annealing results in formation of either $PC_{60}BM$ microcrystals or nanoscale aggregates, depending on the donor polymer employed; in all cases, $PC_{60}BM$ crystallization can be suppressed or totally prevented by a prior illumination step. $PC_{60}BM$ photo-oligomerization is found to be thermally reversible, with a temperature dependence consistent with Arrhenius behavior with an estimated activation energy E_A of 0.96 ± 0.04 eV.

In terms of OSC performance, we show that modest light exposure can substantially enhance the morphological and performance stability of PCDTBT:$PC_{60}BM$ devices under moderate annealing conditions up to 150 h. Mechanistically, we associate this enhancement to the inhibition of $PC_{60}BM$ micro- and nanoscopic crystallization processes upon thermal annealing caused by $PC_{60}BM$ photoinduced oligomerization. This stability enhancement was much less pronounced for PCDTBT:$PC_{70}BM$ devices, consistent with the lower tendency for $PC_{70}BM$ to undergo photoinduced oligomerization. These results are of direct relevance to strategies to optimize, and quantify, the morphological stability of such blend films and organic solar cells, suggesting, for example, that dark 85 °C testing, widely used as a standard PV test condition,[28] may result in greater morphological degradation than the combined light and heat stress more likely under real operating conditions. The observed high sensitivity to even modest light exposure also indicates that light exposure levels must be carefully controlled in studies of the morphology, and the morphological evolution, of polymer:fullerene blend films, topics currently extensively explored in the literature.

METHODS

Sample Preparation. PCDTBT was supplied by 1-Materials, Inc. (M_w ≈ 21.6 kg mol^{-1}; PDI ≈ 5.5). The midpoint T_g of neat PCDTBT was measured as 106 ± 1 °C using differential scanning calorimetry (DSC TA Instruments Q2000) at rate 10 °C/min. PS was purchased from polymer source M_w ≈ 270 kg mol^{-1}; PDI ≈ 1.06). PTB7 was supplied by 1-Materials, Inc. (M_w ≈ 58 kg mol^{-1}; PDI ≈ 2.4). P3HT was supplied by Merck, Inc. with M_w ≈ 34 kg mol^{-1}; and regioregularity (RR) of 94.7%. DPP-TT-T was synthesized at Imperial College London with M_w ≈ 17 kg mol^{-1} and PDI of 6.36. Diiodooctane (DIO), $PC_{60}BM$ and $PC_{70}BM$ were purchased from Sigma Aldrich, Inc.; Nano-C, Inc.; and Solenne BV, respectively.

Morphological Studies. PCDTBT and $PC_{60}BM$ (1:2 weight ratio) was codissolved in 1,2 dichlorobenzene (DCB) and stirred for at least 24 h at 55 °C inside a N_2 glovebox. PS, PTB7, P3HT and DPP-TT-T were individually dissolved in DCB, chlorobenzene CB:DIO 3:97 weight ratio, CB and chloroform CF:DCB (4:1 weight ratio). All solutions (except PTB7:$PC_{60}BM$) were filtered (0.2 μm PTFE filters) before spun cast onto silicon substrates (Compart Technology), resulting in film thickness of 70−120 nm, as determined with a Dektak 6 M profilometer. SiOx substrates were cleaned with nitrogen before use. A fluorescent lamp was used as light source, with light irradiance (≈10 mW/cm^2) and wavelength distribution calibrated with photospectrometer (StellarNet EPP2000). All blend films were illuminated and annealed inside a N_2 filled glovebox with annealing temperatures 80−180 °C measured and calibrated with a surface thermocouple (Kane-May KM330). Blend film morphologies were observed by reflection optical microscope (Olympus BX 41M), equipped with an XY stage and CCD camera (AVT Marlin). *In situ* film thermal annealing was done in N_2 atmosphere with a Linkam microscope heating stage (THMS600). The surface topography of selected annealed films were characterized by atomic force microscopy (Innova, Bruker AXS) in tapping-mode, using super sharp TESP-SS tips. The number density and growth analysis were carried out using Vision Assistant (LabVIEW, National Instruments 8).

Gel Permeation Chromatography. GPC experiments were performed by Agilent Technologies 1200 series GPC with UV/vis detector with detection wavelength of 254 nm, running in chlorobenzene at 80 °C, using two PL mixed B columns in series, and calibrated against narrow polydispersity polystyrene standards. Blend films were kept in the dark or illuminated with fluorescent light for 4 h. Selected illuminated films were subsequently annealed at various temperatures (80−140 °C) for 60 min. The films were redissolved and evaporated in vacuum, with the solids redissolved in chlorobenzene for GPC measurement.

OSC Fabrication and Thermal Stability Studies. ITO glass substrates were cleaned successively with mild detergent solution, acetone and IPA, followed by an oxygen plasma treatment at 100 W for 7 min. A 35 nm thick PEDOT:PSS layer was deposited onto the substrates followed by annealing at 150 °C for 20 min in air. PCDTBT and $PC_{60}BM$ were codissolved in CB with a total solid concentration of 25 mg/mL and a weight ratio of 1:2. Solutions

were stirred in N_2 glovebox at 55 °C for 24 h followed by filtering through a 0.2 μm filter prior spin coating. The active layer film thickness is ≈85 nm thick. All devices were completed by evaporation of 25 nm of calcium and 100 nm of aluminum through a 6-pixel mask with a spatial area of 0.045 cm^2. Device light processing (fluorescent and UV-A light source) was carried out before electrode deposition, followed by the annealing step of the stability test in dark conditions. Both light exposure and annealing steps were conducted in N_2 glovebox. Current density−voltage (J−V) characteristics were measured at selected testing intervals using a Xenon lamp at AM1.5 solar illumination (Oriel Instruments) calibrated to a silicon reference cell with a Keithley 2400 source meter.

Conflict of Interest: The authors declare no competing financial interest.

APPENDIX. The $PC_{60}BM$ thermal decomposition process can be modeled assuming explicit dimer or oligomer populations. Following the treatment of Wang *et al.*[21] (for fullerene C_{60}), the light-induced dimerization and thermally induced decomposition of $PC_{60}BM$ is expressed by a simple rate equation

$$\frac{dD}{dT} = \frac{1}{2}k_P M(t) - k_T D(t) \quad (1)$$

where D and M are dimer and monomer population, k_P is the light-induced dimerization rate, and k_T is the rate constant for dimer thermal dissociation. Given that our thermal annealing experiments were carried in the dark, the first term vanishes and integration of eq 1 becomes simply

$$D(t) = D(t_0)\exp(-k_T t) \quad (2)$$

where $D(t_0)$ and $M(t_0)$ are the dimer and monomer populations following light exposure but prior to thermal stress. Upon dimer thermal dissociation, $M(t)$ increases according to

$$M(t) = M(t_0) + 2 \times D(t_0) \times (1 - \exp(-k_T t)) \quad (3)$$

Combining eqs 2 and 3 gives the population ratio of $PC_{60}BM$ dimers to monomers which can be measured experimentally by GPC and spectroscopy (although the latter can simultaneously cause polymerization and requires a more complex analysis based on eq 1):

$$\frac{D(t)}{M(t)} = \frac{D(t_0)\exp(-k_T t)}{M(t_0) + 2 \times D(t_0) \times (1 - \exp(-k_T t))} \quad (4)$$

The thermal dissociation rate constant k_T was solved numerically for each experimental temperature T and found to be well described by an Arrhenius law, $k_T = k_0 \exp(-E_A/k_B T)$, with activation energy 0.99 ± 0.01 eV [(1.58 ± 0.02) × 10^{-19}J].

Our GPC data indicates the presence of oligomers of 2−3 times the mass of $PC_{60}BM$ monomer, but their exact distribution cannot be determined by resolving the oligomer peak structure. Without assuming an explicit decomposition stoichiometry as done in eq 3, eq 2 can be written in terms of oligomer concentration $O(t)$

$$O(t) = O(t_0)\exp(-k_T t) \quad (5)$$

In the limit of excess of monomer compared to oligomer ($M \gg O$, at all t) and thus little relative change in M, eq 5 yields the approximation

$$k_T \approx -\ln\left(\frac{O(t,T)}{O(t_0)}\right)/t \quad (6)$$

where the relative $O(t)$ can be measured experimentally at a given annealing temperature T (20−140 °C) and constant time t (1 h). E_A is found to be 0.93 ± 0.01 eV, in good agreement with the analysis above, and we thus estimate the activation energy for thermal decomposition of $PC_{60}BM$ in the OSC blend film to be 0.96 ± 0.04 eV [(1.54 ± 0.06) × 10^{-19}J]. The predicted evolution of monomer and oligomer species upon annealing following 4 h of 10 mW/cm^2 fluorescent light illumination is computed in Supporting Information Figure S3.

Acknowledgment. The authors thank Solvay SA and the EPSRC EP/J500021/1, EP/J500239/1 and EP/H040218/1 for financial support. H.C.W. thanks EPSRC for a Doctoral Prize Fellowship Award. The authors thank Alisyn Nedoma and Rajeev Dattani for useful discussions, Shahid Ashraf and Pabitra Shakya for assistance with device fabrication and Martin Heeney for access to the GPC facility.

Supporting Information Available: Thermal properties of PCDTBT and $PC_{60}BM$. Nucleation and growth analysis on PS:$PC_{60}BM$ films. Modeling of the phototransformed and pristine $PC_{60}BM$ population. Additional AFM images on the nanoscale features of PCDTBT:$PC_{60}BM$ films. Compilation of annealed morphologies of a range of OSC donor polymer:$PC_{60}BM$ blend films on SiOx and PEDOT:PSS. Device stability data with continuous irradiation. GPC and morphological characterization of PCDTBT:$PC_{70}BM$. Wavelength spectrum of the fluorescent and UV-A light used. This material is available free of charge *via* the Internet at http://pubs.acs.org.

REFERENCES AND NOTES

1. Kroto, H. W.; Heath, J. R.; O'Brien, S. C.; Curl, R. F.; Smalley, R. E. C60: Buckminsterfullerene. *Nature* **1985**, *318*, 162–163.
2. Kratschmer, W.; Lamb, L. D.; Fostiropoulos, K.; Huffman, D. R. Solid C60: A New Form of Carbon. *Nature* **1990**, *347*, 354–358.
3. Sun, Y.-P.; Ma, B.; Bunker, C. E.; Liu, B. All-Carbon Polymers (Polyfullerenes) from Photochemical Reactions of Fullerene Clusters in Room-Temperature Solvent Mixtures. *J. Am. Chem. Soc.* **1995**, *117*, 12705–12711.
4. Eklund, P. C.; Rao, A. M.; Zhou, P.; Wang, Y.; Holden, J. M. Photochemical Transformation of C60 and C70 Films. *Thin Solid Films* **1995**, *257*, 185–203.
5. Rao, A. M.; Zhou, P.; Wang, K.-A.; Hager, G. T.; Holden, J. M.; Wang, Y.; Lee, W. T.; Bi, X.-X.; Eklund, P. C.; Cornett, D. S.; *et al.* Photoinduced Polymerization of Solid C60 Films. *Science* **1993**, *259*, 955–957.
6. Rao, A. M.; Wang, K.-A.; Holden, J. M.; Wang, Y.; Zhou, P.; Eklund, P. C.; Eloi, C. C.; Robertson, J. D. Photoassisted Oxygen Doping of C60 Films. *J. Mater. Res.* **1993**, *8*, 2277–2281.
7. Jørgensen, M.; Norrman, K.; Gevorgyan, S. A.; Tromholt, T.; Andreasen, B.; Krebs, F. C. Stability of Polymer Solar Cells. *Adv. Mater.* **2012**, *24*, 580–612.
8. Dzwilewski, A.; Wågberg, T.; Edman, L. Photo-Induced and Resist-Free Imprint Patterning of Fullerene Materials for Use in Functional Electronics. *J. Am. Chem. Soc.* **2009**, *131*, 4006–4011.
9. Wang, J.; Enevold, J.; Edman, L. Photochemical Transformation of Fullerenes. *Adv. Funct. Mater.* **2013**, *23*, 3220–3225.
10. Wang, J.; Larsen, C.; Wågberg, T.; Edman, L. Direct UV Patterning of Electronically Active Fullerene Films. *Adv. Funct. Mater.* **2011**, *21*, 3723–3728.

11. Wong, H. C.; Higgins, A. M.; Wildes, A. R.; Douglas, J. F.; Cabral, J. T. Patterning Polymer−Fullerene Nanocomposite Thin Films with Light. *Adv. Mater.* **2013**, *25*, 985–991.
12. Li, Z.; Wong, H. C.; Huang, Z.; Zhong, H.; Tan, C. H.; Tsoi, W. C.; Kim, J. S.; Durrant, J. R.; Cabral, J. T. Performance Enhancement of Fullerene-Based solar Cells by Light Processing. *Nat. Commun.* **2013**, *4*, 2227.
13. Piersimoni, F.; Degutis, G.; Bertho, S.; Vandewal, K.; Spoltore, D.; Vangerven, T.; Drijkoningen, J.; Van Bael, M. K.; Hardy, A.; D'Haen, J.; *et al.* Influence of Fullerene Photodimerization on the PCBM Crystallization in Polymer: Fullerene Bulk Heterojunctions under Thermal Stress. *J. Polym. Sci., Part B: Polym. Phys.* **2013**, *51*, 1209–1214.
14. Granasy, L.; Pusztai, T.; Borzsonyi, T.; Warren, J. A.; Douglas, J. F. A General Mechanism of Polycrystalline Growth. *Nat. Mater.* **2004**, *3*, 645–650.
15. Mandelkern, L. *Crystallization of Polymers, Vol. 2 Kinetics and Mechanism*; Cambridge University Press: Cambridge, U.K., 2004.
16. Wunderlich, B. *Macromolecular Physics Vol.2, Crystal Nucleation, Growth, Annealing*; Academic Press: New York, 1976.
17. Müller, C.; Ferenczi, T. A. M.; Campoy-Quiles, M.; Frost, J. M.; Bradley, D. D. C.; Smith, P.; Stingelin-Stutzmann, N.; Nelson, J. Binary Organic Photovoltaic Blends: A Simple Rationale for Optimum Compositions. *Adv. Mater.* **2008**, *20*, 3510–3515.
18. Beiley, Z. M.; Hoke, E. T.; Noriega, R.; Dacuña, J.; Burkhard, G. F.; Bartelt, J. A.; Salleo, A.; Toney, M. F.; McGehee, M. D. Morphology-Dependent Trap Formation in High Performance Polymer Bulk Heterojunction Solar Cells. *Adv. Energy Mater* **2011**, *1*, 954–962.
19. Wang, T.; Pearson, A. J.; Dunbar, A. D. F.; Staniec, P. A.; Watters, D. C.; Yi, H.; Ryan, A. J.; Jones, R. A. L.; Iraqi, A.; Lidzey, D. G. Correlating Structure with Function in Thermally Annealed PCDTBT:PC70BM Photovoltaic Blends. *Adv. Funct. Mater.* **2012**, *22*, 1399–1408.
20. Lu, X.; Hlaing, H.; Germack, D. S.; Peet, J.; Jo, W. H.; Andrienko, D.; Kremer, K.; Ocko, B. M. Bilayer Order in a Polycarbazole-Conjugated Polymer. *Nat. Commun.* **2012**, *3*, 795.
21. Wang, Y.; Holden, J. M.; Bi, X.-x.; Eklund, P. C. Thermal Decomposition of Polymeric C60. *Chem. Phys. Lett.* **1994**, *217*, 413–417.
22. Germack, D. S.; Chan, C. K.; Hamadani, B. H.; Richter, L. J.; Fischer, D. A.; Gundlach, D. J.; DeLongchamp, D. M. Substrate-Dependent Interface Composition and Charge Transport in Films for Organic Photovoltaics. *Appl. Phys. Lett.* **2009**, *94*, 233303.
23. Germack, D. S.; Chan, C. K.; Kline, R. J.; Fischer, D. A.; Gundlach, D. J.; Toney, M. F.; Richter, L. J.; DeLongchamp, D. M. Interfacial Segregation in Polymer/Fullerene Blend Films for Photovoltaic Devices. *Macromolecules* **2010**, *43*, 3828–3836.
24. He, C.; Germack, D. S.; Joseph Kline, R.; Delongchamp, D. M.; Fischer, D. A.; Snyder, C. R.; Toney, M. F.; Kushmerick, J. G.; Richter, L. J. Influence of Substrate on Crystallization in Polythiophene/Fullerene Blends. *Sol. Energy Mater. Sol. Cells* **2011**, *95*, 1375–1381.
25. Staniec, P. A.; Parnell, A. J.; Dunbar, A. D. F.; Yi, H.; Pearson, A. J.; Wang, T.; Hopkinson, P. E.; Kinane, C.; Dalgliesh, R. M.; Donald, A. M.; *et al.* The Nanoscale Morphology of a PCDTBT:PCBM Photovoltaic Blend. *Adv. Energy Mater* **2011**, *1*, 499–504.
26. Zheng, L.; Liu, J.; Han, Y. Polymer-Regulated Epitaxial Crystallization of Methanofullerene on Mica. *Phys. Chem. Chem. Phys.* **2013**, *15*, 1208–1215.
27. Chen, W.; Xu, T.; He, F.; Wang, W.; Wang, C.; Strzalka, J.; Liu, Y.; Wen, J.; Miller, D. J.; Chen, J.; *et al.* Hierarchical Nanomorphologies Promote Exciton Dissociation in Polymer/Fullerene Bulk Heterojunction Solar Cells. *Nano Lett.* **2011**, *11*, 3707–3713.
28. Reese, M. O.; Gevorgyan, S. A.; Jørgensen, M.; Bundgaard, E.; Kurtz, S. R.; Ginley, D. S.; Olson, D. C.; Lloyd, M. T.; Morvillo, P.; Katz, E. A.; *et al.* Consensus Stability Testing Protocols for Organic Photovoltaic Materials and Devices. *Sol. Energy Mater. Sol. Cells* **2011**, *95*, 1253–1267.
29. De Bettignies, R.; Leroy, J.; Firon, M.; Sentein, C. Accelerated Lifetime Measurements of P3HT:PCBM Solar Cells. *Synth. Met.* **2006**, *156*, 510–513.
30. Bertho, S.; Haeldermans, I.; Swinnen, A.; Moons, W.; Martens, T.; Lutsen, L.; Vanderzande, D.; Manca, J.; Senes, A.; Bonfiglio, A. Influence of Thermal Ageing on The Stability of Polymer Bulk Heterojunction Solar Cells. *Sol. Energy Mater. Sol. Cells* **2007**, *91*, 385–389.
31. Peters, C. H.; Sachs-Quintana, I. T.; Kastrop, J. P.; Beaupré, S.; Leclerc, M.; McGehee, M. D. High Efficiency Polymer Solar Cells with Long Operating Lifetimes. *Adv. Energy Mater* **2011**, *1*, 491–494.
32. Distler, A.; Sauermann, T.; Egelhaaf, H.-J.; Rodman, S.; Waller, D.; Cheon, K.-S.; Lee, M.; Guldi, D. M. The Effect of PCBM Dimerization on the Performance of Bulk Heterojunction Solar Cells. *Adv. Energy Mater* **2014**, *4*, 1–6.
33. Peters, C. H.; Sachs-Quintana, I. T.; Mateker, W. R.; Heumueller, T.; Rivnay, J.; Noriega, R.; Beiley, Z. M.; Hoke, E. T.; Salleo, A.; McGehee, M. D. The Mechanism of Burn-in Loss in a High Efficiency Polymer Solar Cell. *Adv. Mater.* **2012**, *24*, 663–668.
34. Park, S. H.; Roy, A.; Beaupre, S.; Cho, S.; Coates, N.; Moon, J. S.; Moses, D.; Leclerc, M.; Lee, K.; Heeger, A. J. Bulk Heterojunction Solar Cells with Internal Quantum Efficiency Approaching 100%. *Nat. Photonics* **2009**, *3*, 297–302.
35. Wang, D. H.; Kim, J. K.; Seo, J. H.; Park, O. O.; Park, J. H. Stability Comparison: A PCDTBT/PC71BM Bulk-Heterojunction *versus* a P3HT/PC71BM Bulk-Heterojunction. *Sol. Energy Mater. Sol. Cells* **2012**, *101*, 249–255.
36. Rao, A. M.; Menon, M.; Wang, K.-A.; Eklund, P. C.; Subbaswamy, K. R.; Cornett, D. S.; Duncan, M. A.; Amster, I. J. Photoinduced Polymerization of Solid C70 Films. *Chem. Phys. Lett.* **1994**, *224*, 106–112.
37. Collins, B. A.; Li, Z.; McNeill, C. R.; Ade, H. Fullerene-Dependent Miscibility in the Silole-Containing Copolymer PSBTBT-08. *Macromolecules* **2011**, *44*, 9747–9751.
38. Drees, M.; Hoppe, H.; Winder, C.; Neugebauer, H.; Sariciftci, N. S.; Schwinger, W.; Schaffler, F.; Topf, C.; Scharber, M. C.; Zhu, Z.; *et al.* Stabilization of the Nanomorphology of Polymer-Fullerene "Bulk Heterojunction" Blends Using a Novel Polymerizable Fullerene Derivative. *J. Mater. Chem.* **2005**, *15*, 5158–5163.
39. Cheng, Y.-J.; Hsieh, C.-H.; Li, P.-J.; Hsu, C.-S. Morphological Stabilization by In Situ Polymerization of Fullerene Derivatives Leading to Efficient, Thermally Stable Organic Photovoltaics. *Adv. Funct. Mater.* **2011**, *21*, 1723–1732.